

Accurate theoretical analysis of photonic band-gap materials

R. D. Meade, A. M. Rappe, K. D. Brommer, and J. D. Joannopoulos

*Department of Physics and Research Laboratory of Electronics, Massachusetts Institute of Technology,
Cambridge, Massachusetts 02139*

O. L. Alerhand

Bell Communications Research, Red Bank, New Jersey 07701

(Received 10 August 1992; revised manuscript received 11 February 1993)

Two improvements for the solution of Maxwell's equations in periodic dielectric media are introduced, abandoning the plane-wave cutoff and interpolating the dielectric function. These improvements permit the accurate study of previously inaccessible systems. Example calculations are discussed, employing a basis of $\sim 10^6$ plane waves for which these two improvements reduce both the memory and central processing unit requirements by $\sim 10^4$.

The study of electromagnetic radiation in periodic dielectric media has progressed rapidly in the past five years. Initial work focused on materials with three-dimensional symmetry¹⁻⁴ highlighted by the discovery of photonic crystals which possess a photonic band gap.⁵⁻⁷ The scope of inquiry was then broadened to include two-dimensional systems with continuous symmetry in the third dimension⁸⁻¹³ as well as two- and three-dimensional systems whose symmetry is broken by a defect¹⁴⁻¹⁶ or a surface.^{17,18} These investigations revealed that for any photonic crystal with a band gap, a defect can be introduced into the crystal which creates an exponentially localized state at any frequency in the gap. These photonic crystals have a number of interesting physical properties and may also be useful in a number of device applications.^{13,15,16}

Because Maxwell's equations for linear dielectric materials are basically exact, computation has played a critical role in the analysis of photonic crystals. Indeed, although it *appeared* that the fcc structure had a photonic band gap in experiment,² computations of photonic band structures soon showed that it did not.^{3,4} The first structure to have a photonic band gap was found theoretically,⁵ and it was soon confirmed experimentally that a similar structure did have a band gap.⁶ For a number of small systems, it was demonstrated that there was an excellent agreement between theory and experiment.^{6,10,14} All these calculations involved expanding the electromagnetic fields in a basis of plane waves. The reasons for this is that plane waves are complete, can be systematically improved, and do not require any prior knowledge as to the distributions of the fields. However, it was recently shown that this technique suffers from poor plane-wave convergence.^{7,16} For this reason, it has not been possible to apply these methods *accurately* to the important cases of defects in photonic crystals. The purpose of this paper is to introduce a method that leads to dramatic improvements in the computation of the electromagnetic states of photonic crystals and to apply this method to two previously intractable systems.

A single governing equation for electromagnetic states

in photonic crystals can be found by rearranging Maxwell's equations in macroscopic media:

$$\nabla \times \left[\frac{1}{\epsilon(\mathbf{r})} \nabla \times \mathbf{H} \right] = \omega^2 \mathbf{H}. \quad (1)$$

Here, $\epsilon(\mathbf{r})$ is the dielectric function and \mathbf{H} is the magnetic field of an electromagnetic mode of frequency ω . The magnetic field, which must be transverse ($\nabla \cdot \mathbf{H} = 0$), is then expanded in a basis of transverse plane waves, $\mathbf{e}_\lambda e^{i(\mathbf{k}+\mathbf{G})\cdot\mathbf{r}}$, where \mathbf{e}_λ are the unit vectors perpendicular to wave vector $\mathbf{k}+\mathbf{G}$. In this basis, Eq. (1) becomes a matrix eigenvalue equation,

$$\sum_{(G\lambda)'} \Theta_{(G\lambda),(G\lambda)'}^k h_{(G\lambda)'} = \omega^2 h_{(G\lambda)}, \quad (2)$$

where $h_{G\lambda}$ is the coefficient of the plane wave $\mathbf{e}_\lambda e^{i(\mathbf{k}+\mathbf{G})\cdot\mathbf{r}}$, and the matrix Θ is defined by

$$\Theta_{(G\lambda),(G\lambda)'}^k = [(\mathbf{k}+\mathbf{G}) \times \mathbf{e}_\lambda] \cdot [(\mathbf{k}+\mathbf{G}') \times \mathbf{e}_{\lambda'}] \epsilon^{-1}(\mathbf{G}, \mathbf{G}'). \quad (3)$$

In this expression, $\epsilon^{-1}(\mathbf{G}, \mathbf{G}')$ is the inverse of the Fourier transform of the dielectric function $\epsilon(\mathbf{r})$.

The matrix elements in Eq. (3) can be calculated unambiguously when the number of plane waves per polarization (N_{PW}) equals the number of grid points upon which the dielectric function is sampled (N_{FFT}), since the operations of inversion and Fourier transform commute. When the plane-wave set is truncated in order to facilitate convergence, these two operations cease to commute. Ho, Chan, and Soukoulis³ suggest computing an approximation to $\epsilon^{-1}(\mathbf{G}, \mathbf{G}')$ by Fourier-transforming the dielectric function, truncating it, and then inverting the resulting matrix (the Ho, Chan, and Soukoulis method). An alternative approach is to invert the dielectric function in real space, Fourier-transform the inverse, and then truncate the resulting function (the slow method). The convergence properties of eigenstate frequencies as the number of plane waves is increased using these two approaches are depicted in Fig. 1. Since the plane-wave

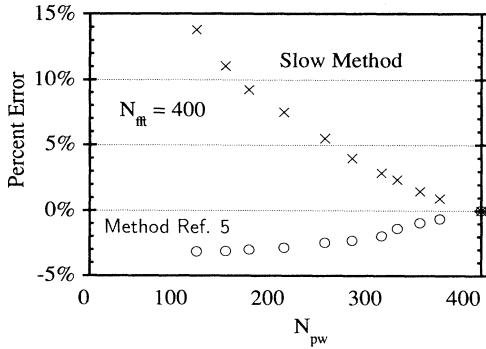


FIG. 1. Rate of convergence of frequency vs N_{PW} for Ho, Chan, and Soukoulis (Ref. 5) and slow methods of calculating ϵ^{-1} . Percent error is defined relative to converged value when $N_{PW} = N_{FFT}$. Calculations were performed on the triangular lattice of air columns (Ref. 12), for the lowest TE band at the M point.

convergence is poor for both these approaches, we are forced to abandon the plane-wave cutoff and choose $N_{FFT} = N_{PW}$. Thus, accurate results can only be obtained in general by using as many plane waves per polarization as dielectric grid points. However, to employ such a scheme, one must develop a method for solving the matrix-eigenvalue equation which scales efficiently with the number of plane waves used. The dominant step in the solution of Eq. (2) is the calculation of matrix-vector products $\Theta \mathbf{H}$ to evaluate the left-hand side of this equation for a trial eigenvector $h_{(G,\lambda)}$.¹⁹ Storage of the matrix Θ requires $(N_{PW})^2$ storage elements, and computation of the matrix-vector product requires $(N_{PW})^2$ multiplications. Building on the ideas of Car and Parrinello²⁰ and Teter, Payne, and Allan²¹ developed for electronic-structure calculations, we have developed a method of computing $\Theta \mathbf{H}$ without storing Θ or explicitly performing the matrix-vector product. Taking the curl of a vector in Fourier space is diagonal in Fourier space. Division by the dielectric function is diagonal in real space, since it affects each real-space location independently. Therefore, we evaluate the left-hand side of Eq. (1) in the following way: We begin with a trial vector in Fourier space and compute its curl. Then, we fast-Fourier-transform (FFT) the result to real space and divide by the dielectric function. Finally, we fast-Fourier-transform this vector back to Fourier space and compute its curl again. The curl and dielectric-function operations are both diagonal in their respective spaces, so the entire calculation requires computer storage of the order N_{PW} . The dominant computational steps are the FFT's, which require CPU operations of the order $N_{PW} \ln(N_{PW})$. For the calculations in this paper which use $\sim 10^6$ plane waves, this new method for solving Maxwell's equations requires approximately 10^4 times less memory and 10^4 times less CPU time. In short, accurate calculations which were impossible to perform have become feasible.

After eliminating the plane-wave cutoff, the main source of inaccuracies is the coarseness of the FFT grid

used to represent the dielectric function. Because the true dielectric function $\epsilon(\mathbf{r})$ is piecewise constant, the representation of $\epsilon(\mathbf{r})$ on the discrete FFT grid ϵ_m is poor along the boundary between dielectrics. A natural attempt to compensate for this coarseness is to smooth ϵ_m at grid points along the boundaries. To do this, we divide the unit cell into equal regions centered about each FFT grid point, which we call pixels. For simplicity, assume $\epsilon(\mathbf{r})$ can have two values ϵ^1 and ϵ^2 . A boundary pixel is one which encloses both ϵ^1 and ϵ^2 . The fractions of the pixel m which contain ϵ^1 and ϵ^2 are designated f_m^1 and f_m^2 , respectively.

We have tested four methods of assigning ϵ_m by systematically increasing N_{FFT} and comparing the convergence rates of the frequencies of a two-dimensional (2D) photonic crystal (see Fig. 2). The first method of assigning ϵ_m was to use a majority rule which does no averaging. In Fig. 2 we see that this method converges slowly. In the second method, ϵ_m is assigned the weighted average of the dielectric constants, $\epsilon_m = \bar{\epsilon}_m \equiv f_m^1 \epsilon^1 + f_m^2 \epsilon^2$. This method accelerates the convergence of TE modes, but slows convergence of TM modes. The third method of interpolating is to perform a weighted average of the inverses of the dielectric constants $\epsilon_m = \bar{\epsilon}_m$, where $1/\bar{\epsilon}_m \equiv f_m^1/\epsilon^1 + f_m^2/\epsilon^2$. Interpolating in this way accelerates convergence for TM modes, but worsens convergence for TE modes. Recalling that the electric fields

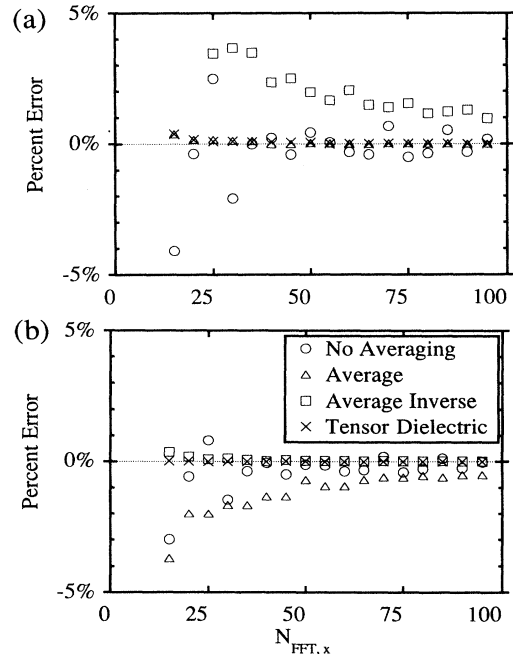


FIG. 2. Rate of convergence of frequency vs $N_{FFT,x}$, the number of FFT points along each side of the unit cell. $N_{FFT} = N_{FFT,x}^2$, for this two-dimensional system. Percent error is defined relative to converged value for large N_{FFT} . Results are shown for convergence of (a) TE and (b) TM modes of the square lattice of dielectric rods (Ref. 14), for the lowest band at the zone edge. TE (TM) modes have electric (magnetic) field oriented along the z direction, normal to the two-dimensional plane.

are primarily parallel to the interface for TE modes and perpendicular for TM modes, it is straightforward to understand these results in terms of effective medium theory²² and to generate a dielectric tensor which works for any polarization. In the fourth and final method, we assign each grid point a dielectric tensor

$$\epsilon_{m,ij} = \bar{\epsilon}_m n_i n_j + \tilde{\epsilon}_m e_{nli} e_{kjl} n_k n_m,$$

where \mathbf{n} is the unit normal to the dielectric interface and e_{ijk} is the Levi-Civita pseudotensor. Interpolating in this way achieves rapid convergence for both TE and TM eigenmodes.

By combining the two techniques described in this paper, we have been able to lower the computational cost per plane wave and the number of plane waves required to perform very accurate photonic calculations. We now discuss the application of these calculational methods to the study of two problems which were completely intractable employing previous methods. The first involves the need for a very accurate determination of the frequency of a defect mode in a 2D lattice.

The system we consider is that studied by McCall *et al.*¹⁴ In their experiment, they study the photonic band gap of the TE modes of a square lattice of dielectric (alumina) cylinders. After removing a single dielectric cylinder, they perform transmission experiments in which it *appears* that this defect creates a localized electromagnetic mode in the gap [Fig. 3(d) of Ref. 14]. We have calculated the eigenvalue spectrum of this defect, employing a 12×12 supercell. For this supercell, we use 32 400 plane waves and calculate 435 bands. For this number of plane waves, we see from Fig. 2(a) that the frequencies are converged better than 0.5%. Hopping between neighboring impurities in the supercell broadens the impurity frequency by 0.003%.

Our calculations reveal that this defect does not create a localized mode in the band gap, but a resonance just above the band edge (see Fig. 3). We can understand the origin of this resonance and find states which are truly lo-

calized by considering the evolution of the eigenmodes as the index of refraction of the defect rod is continuously changed from $\Delta n = 0$ (perfect crystal) to $\Delta n = 2$ (column removed), as shown in Fig. 3. As soon as the index of refraction is less than 3, a state is localized in the gap in a hydrogenic orbit. As Δn is increased between 0 and 0.8, this doubly degenerate mode²³ is swept across the gap (as in Ref. 15). At $\Delta n = 1.4$, a nondegenerate state enters the gap, is swept across, and penetrates the extended states at $\Delta n = 1.8$. Thus, at $\Delta n = 2$, our calculations show that this mode is no longer localized, but is now extended.²⁴ At $\epsilon = 1$, the resonance is 3% above the band edge, which is significantly larger than our computational uncertainty of 0.5%.

Although our calculations show that there is no localized mode for an air defect, the experiments of Ref. 14 do find a peak in the transmission spectrum. This peak is due to the resonance, which is above the global band edge, but below the band edge along the (10) direction in which the experiment was performed. Finally, we note that McCall *et al.* do show the field patterns of a localized state, in Ref. 14, Fig. 4. However, the authors note that this is for a different photonic lattice. For this structure, our calculations do find a state clearly in the center of the gap.

We have also performed calculations on defects in a three-dimensional structure which has been previously studied experimentally and theoretically.¹⁶ This system is particularly challenging because its three-dimensional nature requires a major computational effort. We again employ a supercell method, using a simple cubic supercell consisting of 32 primitive unit cells. For these calculations, we employ $\sim 750\,000$ plane waves for each eigenstate and solve for the lowest 70 bands of the system. The number of FFT points is 12 000 per primitive unit cell. This is 23 points along each direction and computations analogous to those of Fig. 2 show that the frequencies are converged to better than 0.5%. For this size supercell, the hopping between neighboring defects was less

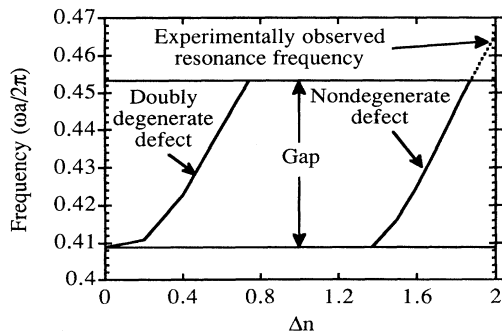


FIG. 3. The evolution of the localized modes of Ref. 14 with decreasing index of refraction of the dielectric cylinder, $\Delta n = n_{\text{alumina}} - n_{\text{defect}}$ ($n_{\text{alumina}} = 3$). The horizontal lines indicate the band edges. In the gap, the frequencies (solid line) are associated with localized states, but after the line punctures the continuum, it becomes a resonance with broadened frequency (dashed line).

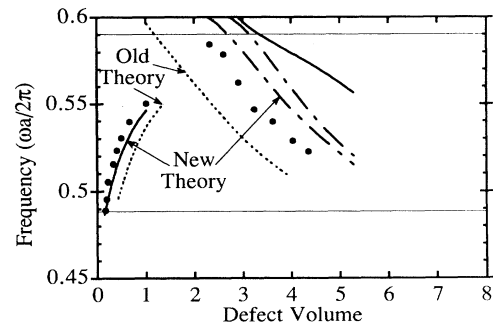


FIG. 4. The frequency of the fully localized states of the three-dimensional photonic band-gap material vs defect size, as discussed in Ref. 16. The dots represent the experimentally measured values, and “old theory” refers to the results of Ref. 16. The solid lines represent nondegenerate modes, whereas the dashed-dotted lines are doubly degenerate. The nondegenerate mode on the left results from an air impurity, while the modes on the right result from a dielectric defect.

than 1% for the dielectric defect and 2% for the air defect.

The results of our improved calculations are shown in Fig. 4. Clearly, there is excellent agreement between theory and experiment for the air defect. However, theory and experiment differ in two ways for the dielectric defect. First, the calculations show that there are three modes which descend, whereas only one peak was identified in the experiments.²⁵ Second, the calculated frequencies are higher than the measured ones, and this difference is larger than the 1% uncertainty of the calculations. The first difference is easy to understand. This is because the experiments were difficult and time consuming to perform, so that only the lowest bound-state mode was identified and reported.²⁶ While the second difference is more puzzling, it is not surprising that the air modes show better agreement than the dielectric modes. The air defect is created by machining away part of the photonic crystal and so it is stable and easy to

create. The dielectric mode, on the other hand, must be inserted into the lattice manually. Because the dielectric sphere is not attached to the lattice, delicate manipulation is required to position the dielectric sphere at the precise site in the lattice at which the defect mode is doubly degenerate.¹⁶ Moreover, this positioning must be maintained over numerous transmission measurements which are required to eliminate sensitivity to antenna position.²⁵ These experimental difficulties introduce an uncertainty into dielectric-defect measurements and may be responsible for the discrepancy between our calculations and the experimental results for this case.

We thank E. Yablonovitch, D. Smith, and S. Schultz for useful discussions. Andrew M. Rappe would like to acknowledge the support of the Joint Services Electronics Program. This work was supported in part by ONR Grant No. 00014-90-J-1370.

-
- ¹E. Yablonovitch, *Phys. Rev. Lett.* **58**, 2059 (1987).
²E. Yablonovitch and T. J. Gmitter, *Phys. Rev. Lett.* **63**, 1950 (1989).
³K. M. Leung and Y. F. Liu, *Phys. Rev. Lett.* **65**, 2646 (1990).
⁴Ze Zhang and Sashi Satpathy, *Phys. Rev. Lett.* **65**, 2650 (1990).
⁵K. M. Ho, C. T. Chan, and C. M. Soukoulis, *Phys. Rev. Lett.* **65**, 3152 (1990).
⁶E. Yablonovitch, T. J. Gmitter, and K. M. Leung, *Phys. Rev. Lett.* **67**, 2295 (1991).
⁷H. S. Sozuer, J. W. Haus, and R. Inguva, *Phys. Rev. B* **45**, 13962 (1992).
⁸M. Plihal, A. Shambrook, A. A. Maradudin, and P. Sheng, *Opt. Commun.* **80**, 199 (1991).
⁹M. Plihal and A. A. Maradudin, *Phys. Rev. B* **44**, 8586 (1991).
¹⁰W. Robertson, G. Arjavalingam, R. D. Meade, K. D. Brommer, A. M. Rappe, and J. D. Joannopoulos, *Phys. Rev. Lett.* **68**, 2023 (1992).
¹¹P. Villeneuve and M. Piche, *Phys. Rev. B* **46**, 4973 (1992).
¹²R. D. Meade, K. D. Brommer, A. M. Rappe, and J. D. Joannopoulos, *Appl. Phys. Lett.* **61**, 495 (1992).
¹³D. L. Bullock, C. C. Shih, and R. S. Marguiles, *JOSA B* **10**, 399 (1993).
¹⁴S. L. McCall, P. M. Platzman, R. Dalichaouch, D. Smith, and S. Schultz, *Phys. Rev. Lett.* **67**, 2017 (1991).
¹⁵R. D. Meade, K. D. Brommer, A. M. Rappe, and J. D. Joannopoulos, *Phys. Rev. B* **44**, 13772 (1991).
¹⁶E. Yablonovitch, T. J. Gmitter, R. D. Meade, K. D. Brommer, A. M. Rappe, and J. D. Joannopoulos, *Phys. Rev. Lett.* **67**, 3380 (1991).
¹⁷R. D. Meade, K. D. Brommer, A. M. Rappe, and J. D. Joannopoulos, *Phys. Rev. B* **44**, 10961 (1991).
¹⁸W. Robertson, G. Arjavalingam, R. D. Meade, K. D. Brommer, A. M. Rappe, and J. D. Joannopoulos, *Opt. Lett.* **18**, 529 (1993).
¹⁹G. Golub and C. Van Loan, *Matrix Computations* (Johns Hopkins University Press, Baltimore, MD, 1989), p. 440.
²⁰R. Car and M. Parrinello, *Phys. Rev. Lett.* **55**, 2471 (1985).
²¹M. P. Teter, M. C. Payne, and D. C. Allen, *Phys. Rev. B* **40**, 12255 (1989).
²²D. E. Aspnes, *Am. J. Phys.* **50**, 104 (1982).
²³After performing these computations, we became aware that this doubly degenerate mode has been observed experimentally. D. Smith and S. Schultz (private communications).
²⁴Further calculations show that this result is quite robust. In particular, the state is a resonance even if the background dielectric is chosen to be 1.04, the value for styrofoam (which was employed in the experiments). Furthermore, the state is also a resonance if the lattice constant is chosen to be 1.25 cm, a more accurate value (Ref. 23) than the 1.27 cm quoted in Ref. 14.
²⁵Earlier calculations, employing the traditional methods, also found the presence of three modes. While it was previously unclear whether these modes were an artifact of the computational method, there is no doubt in the present scheme.
²⁶E. Yablonovitch (private communication).